ARTICLE

Graphene Textile Strain Sensor with Negative Resistance Variation for Human Motion Detection

Zhen Yang,[†,‡,#] Yu Pang,[†,‡,#] Xiao-lin Han,[†,‡] Yifan Yang,[†,‡] Jiang Ling,[†,‡] Muqiang Jian,[§] Yingying Zhang,[§] Yi Yang,*[,†,‡] and Tian-Ling Ren*[,†,‡]

[†]Institute of Microelectronics, Tsinghua University, Beijing 100084, China
[‡]Beijing National Research Center for Information Science and Technology (BNRist), Tsinghua University, Beijing 100084, China
[§]Department of Chemistry and Center for Nano and Micro Mechanics (CNMM), Tsinghua University, Beijing 100084, China

Ⓢ *Supporting Information*

ABSTRACT: Recently, wearable devices have been attracting significantly increased interest in human motion detection and human physiological signal monitoring. Currently, it is still a great challenge to fabricate strain sensors with high performance and good fit to the human body. In this work, we fabricated a close-fitting and wearable graphene textile strain sensor based on a graphene textile without polymer encapsulation. Graphene oxide acts as a colorant to dye the polyester fabric and is reduced at high temperature, which endows the graphene textile strain sensor with excellent performance. Compared with the previously reported strain sensors, our strain sensor exhibits a distinctive negative resistance variation with increasing strain. In addition, the sensor also demonstrates fascinating performance, including high sensitivity, long-term stability, and great comfort. Based on its superior performance, the graphene textile strain sensor can be knitted on clothing for detecting both subtle and large human motions, showing the tremendous potential for applications in wearable electronics.

KEYWORDS: graphene textile strain sensor, negative resistance variation, colorant, human motions, resistance models
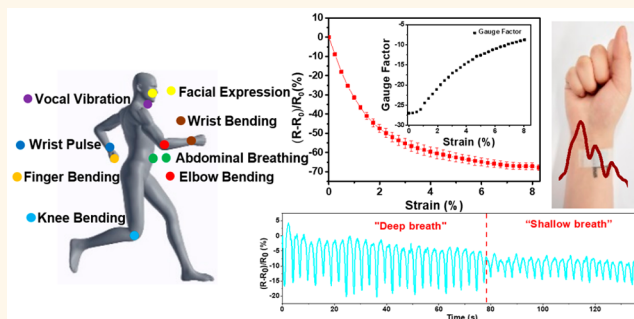
Wearable and flexible electronic devices have attracted tremendous attention in recent years due to their friendly contact with human body and stable monitoring capabilities.[1−6] Strain sensors are fundamental components of electronic devices, and the preparation of innovative strain sensors is critical to the development of wearable electronic devices. In addition, strain sensors play significant roles in biomedical electronics, which can monitor various body signals including physical, chemical, and biological signals.[7−10] Many vital factors have been taken into account to evaluate the performance of strain sensors, among which the sensing materials and device structures may dominantly affect the sensitivity, stretchability, response time, long-term stability, and durability. Therefore, numerous efforts have been made to develop advanced fabrication techniques and materials to improve the performance of strain sensors.

To date, strain sensors based on various typical micro/nanostructures have been fabricated, employing nanomaterials as conducting elements due to their outstanding electrical, mechanical, optical, and chemical properties.[11−14] Especially, graphene has been extensively studied for strain-sensing

applications.[15−18] Chen *et al.* developed a macroscopic 3D graphene foam structure by a template-directed CVD technique. The composite integrated graphene foam with a polymer served as a flexible, foldable, and stretchable conductor that could be stretched to 95%.[19] Yan *et al.* fabricated a strain sensor with three-dimensional macroporous nanopapers composed of crumpled graphene and nanocellulose, embedded in a stretchable elastomer matrix. The sensor based on stretchable nanopapers exhibited a gauge factor of 7.1 at 100% strain and allowed all-directional sensing, which was critical for human motion detection.[20]

In general, the prepared sensing elements are encapsulated in polymer materials to fabricate strain sensors,[21−24] which has many disadvantages, such as low fit with the human body, unsatisfying comfort, and a complex preparation process. However, we fabricate a graphene textile strain sensor based on
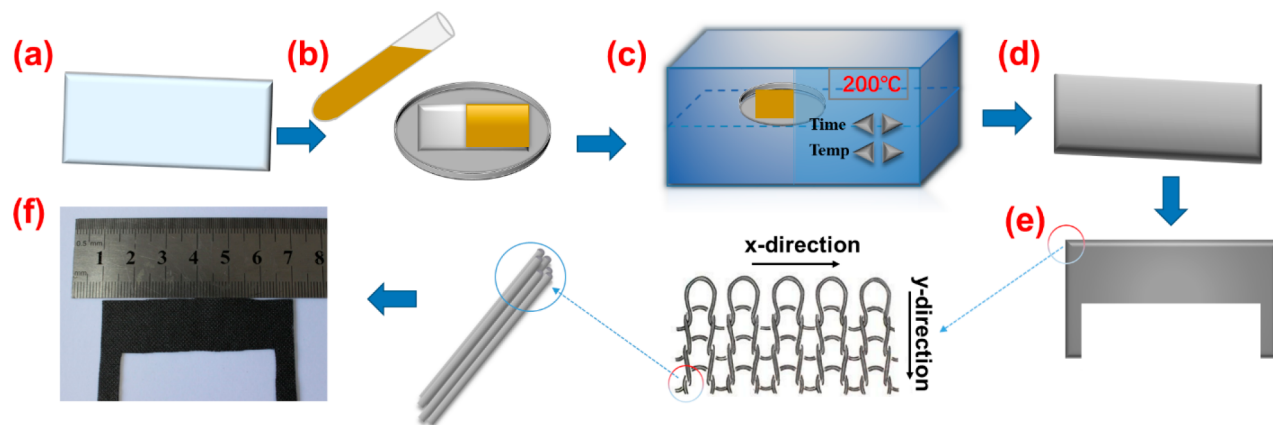
Figure 1. Fabrication process and structure of the graphene textile strain sensor. (a−e) Fabrication process of the graphene textile strain sensor. (d) Woven structure of the graphene textile. (f) Photograph of the graphene textile strain sensor.
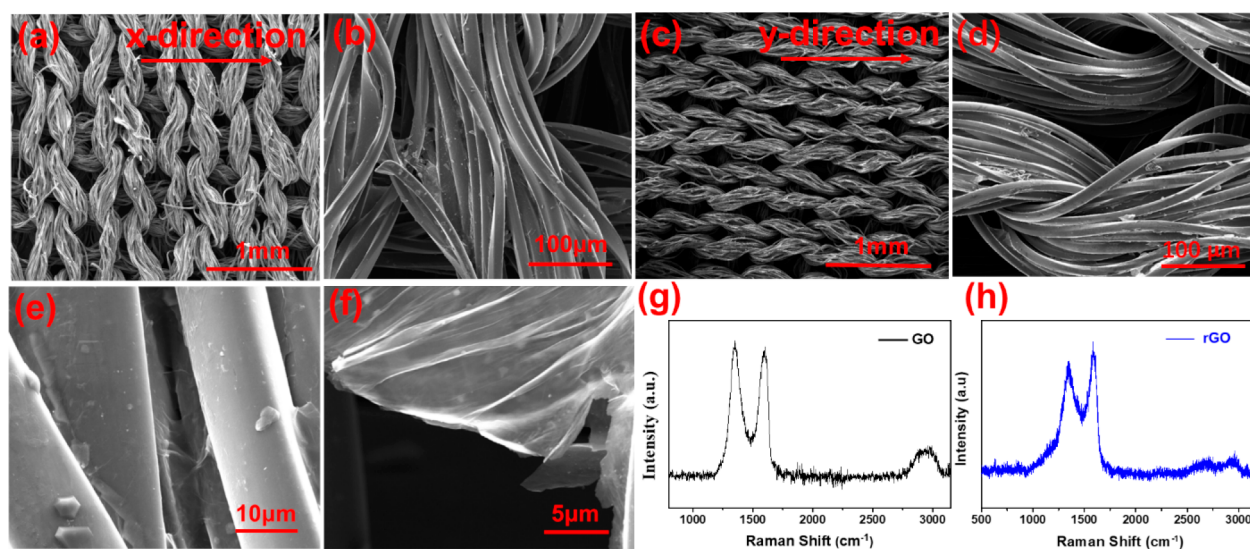

Figure 2. Characterizations of the graphene textile. (a) SEM image of the graphene textile in the *x*-direction. (b) Entire wire in the *x*-direction. (c) SEM image of the graphene textile in the *y*-direction. (d) Magnified SEM image of the whole wire in the *y*-direction. (e) Connected graphene sheets in the same wire. (f) SEM image of graphene sheets. (g, h) Raman spectra of GO and rGO.

polyester fabrics without polymer material encapsulation, which demonstrates more close-fitting with the human body. In this report, graphene oxide acts a colorant to dye the polyester fabric, fabricating a negative resistance variation graphene textile strain sensor. Particularly, the graphene textile contains vertical and horizontal fibers and forms a conductive network during stretching, showing different tensile properties. The graphene textile strain sensor exhibits combined superiority of wide strain range up to 15%, high sensitivity, and long-term stability, which can be knitted directly on clothing for monitoring real-time human physiology activities. The graphene textile strain sensor without polymer material encapsulation could be simply extended to other woven fabrics, providing a method for the low-cost and scalable fabrication of wearable strain sensors.

RESULTS AND DISCUSSION

The fabrication process of the integrated graphene textile strain sensor is illustrated in Figure 1. The sensor was made of polyester fabrics. First, we cropped many 6 cm × 1.5 cm samples along the *x*-direction and *y*-direction polyester fabric (Figure 1a). The polyester fabric was dipped in a graphene

oxide (GO) dispersion for 3 min and baked under an infrared lamp for 20 min (Figure 1b). The above process was repeated three times. After that, as shown in Figure 1c, the polyester fabric was placed in a furnace at 200 °C for 2 h in order to reduce the GO sheets to graphene sheets. The graphene textile is shown in Figure 1d. The electrodes of the graphene textile strain sensor can be obtained directly by cutting two strips from the polyester fabric instead of fabricating them by copper foil and silver paste (Figure 1e). Figure 1f shows a photograph of the graphene textile strain sensor. To confirm the mechanism of the sensor, the graphene textile was encapsulated with an elastic silicone, polydimethylsiloxane (PDMS), fabricating the graphene textile PDMS strain sensor. The fabrication process of the graphene textile PDMS strain sensor is shown in Figure S1 (Supporting Information).

The characterizations of the graphene textile are shown in Figure 2. Figure 2a shows a typical scanning electron microscopy (SEM) image of the graphene textile strain sensor in the *x*-direction. SEM images at different magnifications and angles were observed to further analyze the morphology of the graphene textile. Figure 2b shows a magnified SEM image of an entire wire in the *x*-direction. Figure 2c presents a SEM image
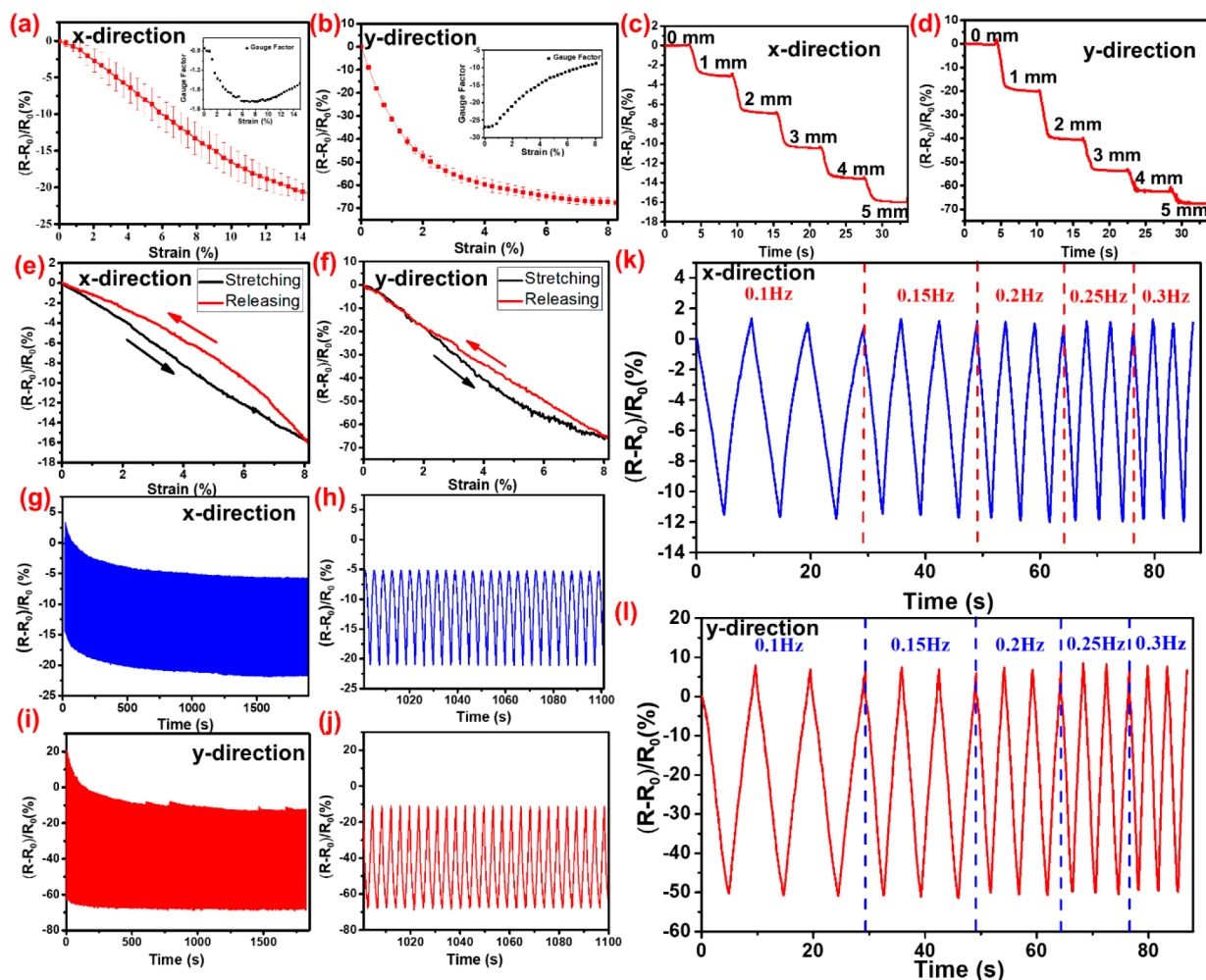
Figure 3. Performance of the graphene textile strain sensor. (a) Relative resistance changes of the graphene textile strain sensor *versus* the applied strain in the *x*-direction. (b) Relative change in resistance *versus* strain in the *y*-direction stretching. Relative resistance change−time curve at different strains in the (c) *x*-direction and (d) *y*-direction, respectively. Hysteresis of the relative resistance change during stretching/releasing in the (e) *x*-direction and (f) *y*-direction, respectively. Performance of the sensor under 500 cycles of tensile loading in the (g) *x*-direction and (i) *y*-direction, respectively. (h) Magnified cycles with *x*-direction stretching. (j) Magnified cycles with *y*-direction stretching. Relative resistance variation under cyclic stretching/releasing at frequencyies of 0.1, 0.15, 0.2, 0.25, and 0.3 Hz in the (k) *x*-direction and (l) *y*-direction.

of the graphene textile in the *y*-direction, and Figure 2d shows a whole wire in the *y*-direction. The graphene sheets were homogeneously penetrated into the graphene textile, forming crosswise graphene textile conductive networks. Due to the special structure, the graphene textile conductive networks can withstand both vertical and horizontal tensile deformation, exhibiting different tensile properties. Figure 2a and c show a weft-knit polyester fabric, revealing the woven structure of the polyester fabric consisted of continuous unit coil sets of fibers. A high-magnification view of the graphene textile indicates that the graphene sheets connect many fibers in the same wire (Figure 2e). Figure 2f shows a magnified image of the graphene sheets. The cross-sectional SEM images of the graphene textile exhibit a loose interlayer structure consisting of vertical and horizontal fibers (Figure S2). The graphene sheets are immobilized on the surface of the graphene textile, which endows the fibers with a closer connection under mechanical deformation. The Raman spectrum of GO is presented in Figure 2g. The Raman spectrum of the rGO (reduced graphene oxide) presents typical graphene peaks, which consist of a G-band at 1593 cm^{-1} and a D-band at 1350

cm^{-1} [25] (Figure 2h). The D-band indicates the existence of defects. The G-band is associated with crystalline sp^2 carbon.[26] The existence of a relatively broad and weak 2D-band at 2750 cm^{-1} also reveals the defects of the graphene textile.[27]

The graphene textile strain sensor exhibits a negative resistance variation and different tensile performance. Figure 3a shows a typical plot for the graphene textile strain sensor with *x*-direction stretching, where R_0 and R represent the initial and real-time resistances, respectively. The sample-to-sample variation of graphene textile strain sensors (Figure 3a) indicates the consistency of different samples and great repeatability of the fabrication process. The sensor displays a negative resistance variation and a maximum gauge factor (GF) of −1.7 within a 15% strain range during *x*-direction stretching, demonstrating a wide strain range. Figure 3b presents the performance of the graphene textile strain sensor with *y*-direction stretching, with an 8% strain range and a maximum GF of −26, which also exhibits a negative resistance variation. From Figure 3a and b, the graphene textile strain sensor shows a wide strain range with *x*-direction stretching and high sensitivity with *y*-direction stretching. To further
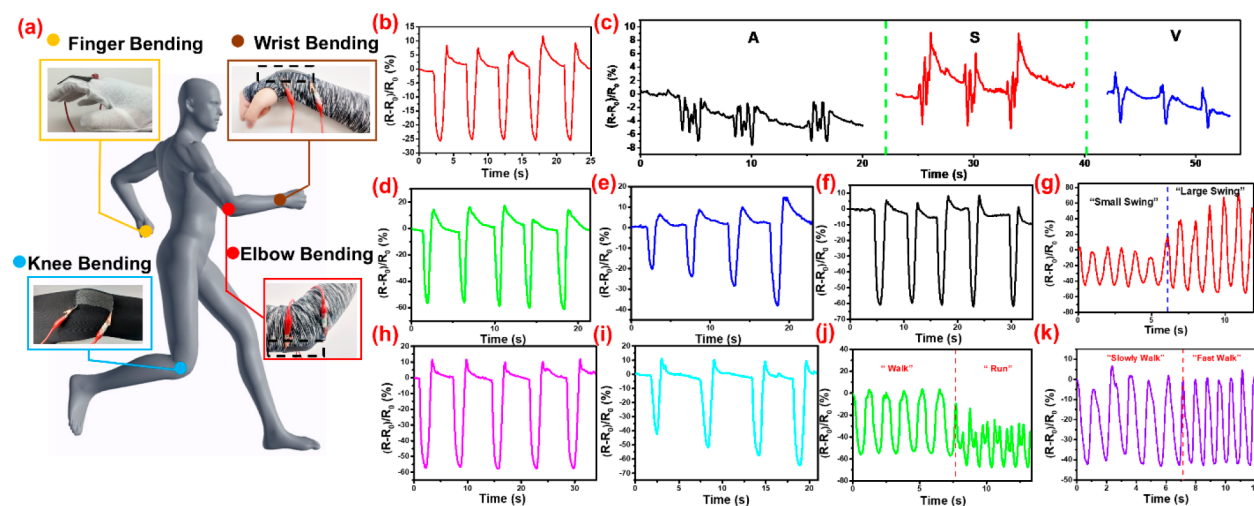
Figure 4. Detection of various human motions using the wearable graphene textile strain sensor. (a) Overview of sensing locations. (b) Corresponding signals of the bending of the wrist. (c) Detection of writing English letters. (d) Signals with the bending of a finger at a certain angle. (e) Relative change in resistance under different finger bending angles. (f) Bending of the elbow joint. (g) Elbow swing with different amplitudes. (h) Bending of a knee joint. (i) Knee bending with different angles. (j) Different signals with walking and running. (k) Walking at different frequencies.

verify the stretching mechanism, PDMS were used to encapsulate the graphene textile, fabricating a graphene textile PDMS strain sensor. The performance of the sensor is demonstrated in Figure S3. It can be observed that the sensor has a positive resistance variation, which is opposite of the strain sensor without PDMS encapsulation. The PDMS solidifies the woven structure of the graphene textile and prevents the formation of nodes between the horizontal and vertical wires, which renders the graphene textile PDMS strain sensor similar to the reported resistive-type strain sensor.[28−32] As shown in Figure 3c and d, the relative resistance changes *versus* time curve during 5 mm distance stretching demonstrates that the signals remain stable without distinct drifts during each period. It is also observed that the relative changes in resistance with *x*-direction and *y*-direction stretching are different along with the 1 mm stretching distance in each step. Figure 3e and f show the hysteresis of relative resistance change during stretching/releasing in the *x*-direction and *y*-direction, respectively. As shown in Figure 3g and i, the electrical response of the graphene textile strain sensor exhibits excellent stability and durability during 500 cycles of 7.5% strain in the *x*-direction and 500 cycles of 5% strain in the *y*-direction. Figure 3h and j show the magnified cycles. The performance testing of the relative resistance change *versus* strain after 0, 100, 200, 300, 400, and 500 cycles is shown in Figure S4, confirming the stability of the sensor. In order to further verify the stability of the graphene textile strain sensor, we washed the sensors with deionized water and laundry liquid (Figure S5). It can be clearly observed that the sensors did not fade by comparing the color of the liquid before and after washing. In addition, the electrical testing of the washed graphene textile strain sensor is demonstrated in Figure S6. The performance degradation of the graphene textile strain sensor is not obvious after washing. It could be inferred that the graphene oxide acts as a colorant to dye the polyester fabric, endowing the sensor with excellent performance. The performance change of the graphene textile PDMS strain sensor with the washing process is shown in Figure S7, and the performance degradation of the sensor is not obvious due to the protection by PDMS. As shown in Figure 3k and l, the

relative resistance changes of the graphene textile strain sensor exhibits almost no frequency dependence within the tested frequency range from 0.1 to 0.3 Hz in the *x*-direction and *y*-direction. Figure S8 shows the relative resistance change of the sensor under cyclic stretching−releasing with a different strain range in the *x*-direction, which is consistent with the result shown in Figure 3a. Figure S9 shows the multicycles under different strain ranges in the *y*-direction and the relative resistance change consistent with the GF in Figure 3b. From the above, the graphene textile strain sensor shows a negative resistance variation, high sensitivity, wide range strain, and excellent durability. The comparison of performance between our strain sensors with other traditional ones is listed in Table S1. It clearly shows a negative resistance variation performance of our sensors.

Because of the facile interaction with the human body, high sensitivity, and wide working range, the graphene textile strain sensor can be knitted on clothing for tremendous potential applications in wearable devices. Figure 4a shows an overview of sensing locations, indicating the high adhesion with the human body and wearable features of the graphene textile strain sensor. In Figure 4a, the sensor was mounted on different joints, such as the wrist, knee, elbow, and finger, detecting large motions. The sensor also monitors subtle motions, such as facial expressions, breathing, pulse, writing, and vocal vibration. As shown in Figure 4b, a wrist guard integrated with a graphene textile strain sensor can monitor wrist movement, such as bending/recovering. In addition, the sensor even could be attached on the wrist for detecting handwriting, including the English alphabet and Chinese characters. Figure 4c presents the relative resistance change with different English letters, such as "A", "S", and "V"; all English letters are demonstrated in Figure S10, and the Chinese characters for 1 to 10 and different English names are presented in Figure S11. We also knitted the graphene textile strain sensor on a single glove to monitor its response toward the bending of a finger. The relative resistance change is uniform when the finger is bent at a certain angle (Figure 4d), and the angles of the finger bending could be precisely tracked by monitoring the relative change in resistance (Figure 4e). To detect the swing of the
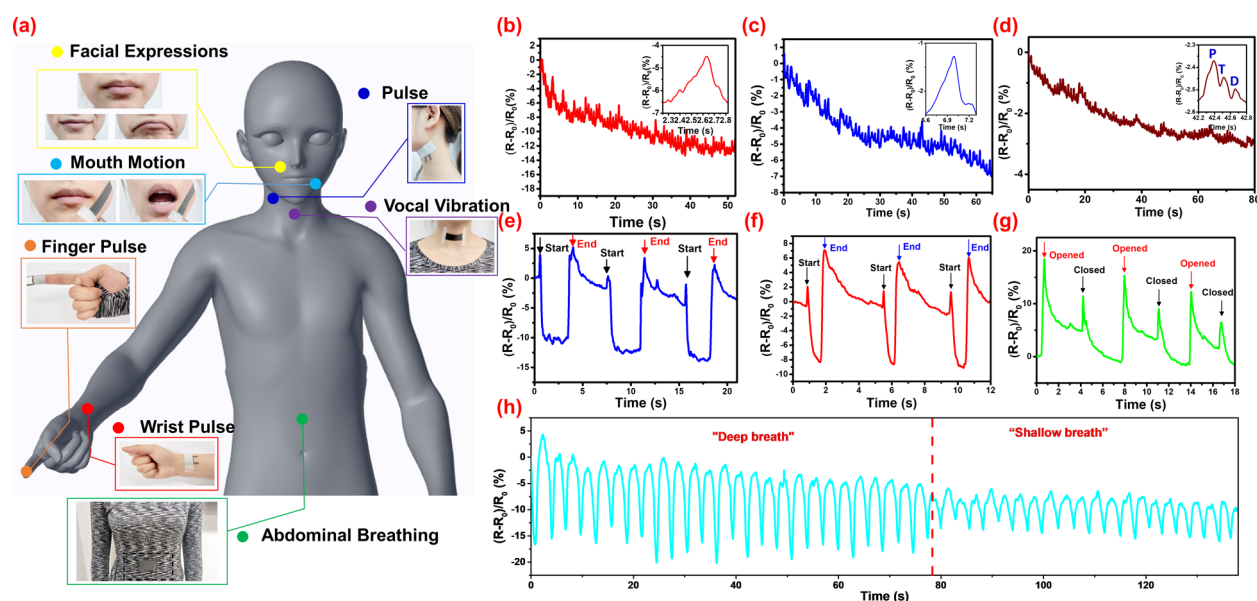
Figure 5. Applications of the wearable graphene textile strain sensors for detecting various subtle human motions. (a) Schematic illustration of the sensor attached to different parts for detecting subtle human motions. (b) Signal of a finger pulse; the inset is a single pulse. (c) Signal of a pulse; the inset is a single signal. (d) Wrist pulse signal; the inset is a single pulse that contains characteristic peaks called P-wave, T-wave, and D-wave. (e) Signal of laughing. (f) Signal of crying. (g) Relative resistance changes during opening and closing the mouth. (h) Detection of respiration rate with different breath modes.

elbow while walking, we mounted the sensor on the elbow joint. Figure 4f shows the relative change in resistance when bending the elbow at a certain angle, and Figure 4g demonstrates that the relative resistance changes are various under a small swing and a large swing. The graphene textile strain sensor was knitted on the trousers to detect every movement of the knee. The relative resistance change is uniform when the knee is bent at a certain angle (Figure 4h), and the knee bending with different angles also indicates a high sensitivity of the sensor (Figure 4i). Furthermore, we also monitored different motion conditions, such as walking, running, and walking frequency. It could be clearly observed that waveforms for walking and running are different (Figure 4j) and the variety in frequency of a slow walk and fast walk (Figure 4k).

Figure 5a demonstrates a schematic illustration of the graphene textile strain sensor attached to different parts for detecting subtle human motions, such as muscle movements, pulse, respiration, and facial expressions. Pulse is a very important physiological signal for systolic and diastolic blood pressure as well as heart rate. The graphene textile strain sensor could be used for detecting the pulse. Finger pulse is demonstrated in Figure 5b, and a single pulse is presented in the inset. In addition, the graphene textile strain sensor was placed on the neck to detect real-time pulse changes (Figure 5c), and the inset shows a single pulse wave. The sensor was attached to a wrist band for detecting real-time pulse signals under relaxation conditions (Figure 5d). It clearly displays repeatable and regular pulse shapes during relaxation with a frequency of 70 beats min^{-1}. As shown in the inset, the close-up of a single pulse peak clearly reveals typical characteristics of the pulse waveform, namely, the percussion wave (P-wave), tidal wave (T-wave), and diastolic wave (D-wave),[33] demonstrating the high sensitivity of the sensor. The graphene textile strain sensor was attached on the skin near the mouth to detect facial expressions of crying and laughing, and the plots

of relative resistance change *versus* time for laughing and crying are demonstrated in Figure 5e and f, respectively. Figure 5g presents the relative changes in resistance when the mouth is open and closed. The graphene textile strain sensor was attached at the throat for recognizing the muscle motion induced by speaking different words, and signals with different words are demonstrated in Figure S12. It could be seen that the single word waveform is apparently different and the repeatability of each cycle is fine. Respiration rate is detected by knitting the graphene textile strain sensor on the clothing near the abdomen, as shown in Figure 5h. The respiration cycles consist of two different modes, deep breathing and shallow breathing. The above results indicate the excellent performance of the graphene textile strain sensors for detecting human motions.

In order to understand the working mechanism of the graphene textile strain sensors, we tracked the structure evolution by SEM during the original status (Figure 6a) and small *x*-direction loading status (Figure 6b) and large *x*-direction loading status (Figure 6c). Figure 6d, e, and f show the structure change during different strain forces in the *y*-direction. The initial status of the graphene textile is shown in Figure 6a and d. It can be obviously observed that a single wire consists of many loose fibers, and the interlock-stitch structure consists of horizontal and vertical wires. As shown in Figure 6b and c, the fibers in the same wire become more compact, and the wire-to-wire contacts become closer together and form a node. The existence of nodes ensures integrity of the woven structure and prevents the rupture of the conductive pathways under a large deformation. More importantly, the structure of the sensor translates into a conductive network during stretching, which results in a decrease of the entire resistance. In addition, the width of the gaps increases with the increase in strain, which contributes to the increase of the resistance. Due to the obvious change of the conductive structure, the bulk resistance still decreases with stretching. The size of gaps is
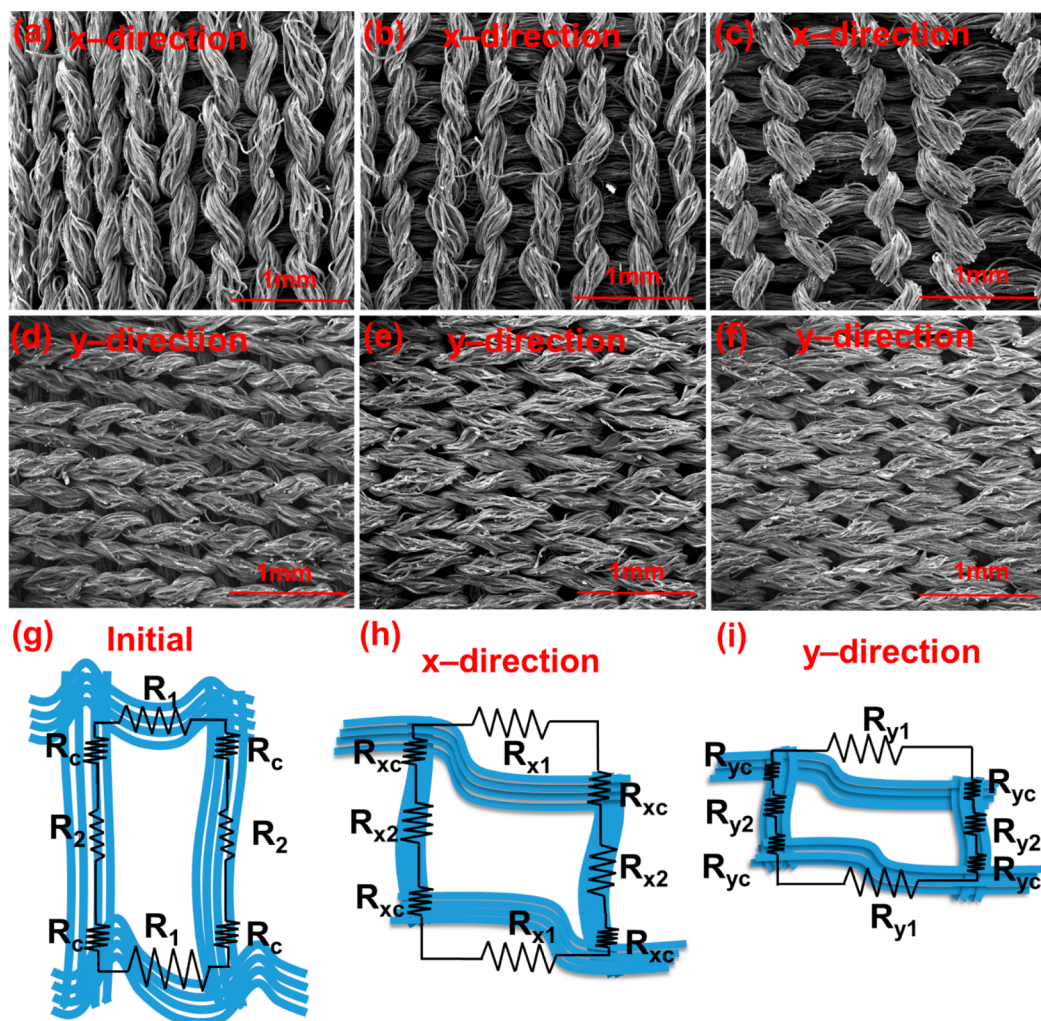
Figure 6. Mechanism of the graphene textile strain sensor. SEM image of a graphene textile strain sensor during (a) initial loading in the *x*-direction, (b) small loading in the *x*-direction, (c) large loading in the *x*-direction. (d–f) SEM images of the graphene textile strain sensor during different loading in the *y*-direction: (d) initial status, (e) small loading, (f) large loading. (g) Initial status resistance model of the sensor without any loading. (h) Resistance model with *x*-direction stretching. (i) Resistance model with *y*-direction stretching.

different under stretching in the *x*- and *y*-directions, which contributes to the different change in resistance.

To understand the relationship between the structural deformation and the relative resistance change, we developed simple resistance models to describe this relationship. In the initial status (Figure 6g), the current is divided into two paths through this resistance unit which flows through $R_1-R_c-R_2-R_c$ and $R_c-R_2-R_c-R_1$ separately. The total initial resistance (R_0) could be calculated as

$$R_0 = \frac{(R_1 + R_2 + 2R_c)}{2} \quad (1)$$

where R_1 and R_2 are the resistances of the graphene textile in *x*-direction and *y*-direction, respectively. R_c is the contact resistance between horizontal and vertical wires without any applied strain. In the initial status, the horizontal and vertical woven wires have a small gap at the junction or a little contact with each other, which leads to a very large contact resistance. Compared to the contact resistance R_c, the resistances R_1 and R_2 can be neglected. Thus, eq 1 can be approximated as $R_0 = R_c$.

The structure would be translated into a conductive network during *x*-direction stretching, which leads to the formation of nodes between the horizontal and vertical wires. The fibers on the same wire become closer, which decreases the resistance of the wire itself. The formation of network nodes leads to a decrease in the contact resistance. As shown in Figure 6h, the resistance unit is divided into two parts ($R_{x1}-R_{xc}-R_{x2}-R_{xc}$ and $R_{xc}-R_{x2}-R_{xc}-R_{x1}$) and the two components are connected in parallel. Therefore, the resistance with *x*-direction stretching (R_x) could be demonstrated as

$$R_x = \frac{R_{x1} + R_{x2} + 2R_{xc}}{2} \quad (2)$$

where R_{x1}, R_{x2}, and R_{xc} are the resistances of graphene textile in the *x*-direction and *y*-direction during *x*-direction stretching and the contact resistance between the horizontal wire and vertical wire, respectively. The fibers in the same wire become more compact with *x*-direction stretching, resulting in the decrease of R_{x1} and R_{x2}. At the same time, the contact resistance R_{xc} also decreases due to the formation of nodes. Therefore, the resistance R_x with *x*-direction stretching is less than the initial resistance R_0, indicating the negative resistance

variation of the sensor. Similarly, in Figure 6i, the resistance with y-direction stretching (R_y) could also be summed up as

$$R_y = \frac{R_{y1} + R_{y2} + 2R_{yc}}{2} \tag{3}$$

where R_{y1}, R_{y2}, and R_{yc} are the horizontal and vertical resistances and the contact resistance during y-direction stretching, respectively. Similar to x-direction stretching, the resistance R_y also decreases with y-direction stretching. The difference between Figure 6h and i is caused by the size of gaps during stretching. The density of the conductive units is different during the x- and y-direction stretching process, resulting in the different resistance variation. These resistance models reasonably explain the relationship between structural deformations and the relative resistance change.

CONCLUSIONS

In summary, we have fabricated a wearable graphene textile strain sensor with negative resistance variation through a simple thermally reduced GO. The graphene oxide acts as a colorant to dye the polyester fabric, endowing the graphene textile strain sensor with excellent performance. The maximum GF of the sensor is −26 in the strain range of 8% under y-direction stretching and −1.7 in the strain range of 15% in the x-direction. The variation of horizontal and vertical interwoven structure contributes to the distinctive direction sensitivities of the sensor. Furthermore, the graphene textile strain sensor has a high durability and stability. The graphene textile strain sensor could be knitted directly on clothing for both large and subtle human motion detection, such as the bending of joints, facial expressions, pulse monitoring, and hand-writing recognition, indicating the tremendous potential applications as wearable electronics. The sensor without PDMS encapsulation demonstrates a high close-fitting property, and the performance of the sensor hardly changes after washing, which enables perfect integration with clothing. It can be used to produce wearable electronics on clothes, which can truly achieve real-time human motion detection.

MATERIALS AND METHODS

Preparation of the Graphene Textile Strain Sensor. The GO was purchased from Nanjing XFNANO Materials Tech Co., Ltd. The average diameter of the dispersed GO sheet is larger than 500 nm, and the concentration is 2 mg mL^{-1}. The polyester fabric was cut into rectangles and then immersed in a GO solution for 3 min and dried under an infrared lamp at 50 °C for 20 min. Afterward, the above experimental procedure was repeated three times. After completing the above experimental process, the polyester fabric was put in a furnace at 200 °C for 2 h, and GO was reduced to graphene sheets.

Preparation of the Graphene Textile PDMS Strain Sensor. After the preparation of the graphene textile, it was connected to copper foil at both ends with silver paste and put on a PDMS substrate (a 10:1 mixture of PDMS liquid and a plasticizer); then liquid PDMS was dropped on the surface to encapsulate the strain sensor. Finally, the sample was cured at 60 °C for 12 h.

Characterization of the Graphene Textile. The morphology of graphene textile was characterized by field emission SEM (Quanta FET 450). The Raman spectra were obtained with a Lab RAM HR Evolution (JY-HR800) with a laser excitation wavelength of 514 nm and power of 50 mW at room temperature. The electromechanical properties of the strain sensor were measured with a testing machine (Shimadzu AGS-X) and digital electrometer (Rigol DM3068).

ASSOCIATED CONTENT

Ⓢ Supporting Information

The Supporting Information is available free of charge on the ACS Publications website at DOI: 10.1021/acsnano.8b03391.

Additional information (PDF)

AUTHOR INFORMATION

Corresponding Authors
*E-mail: yiyang@tsinghua.edu.cn.
*E-mail: RenTL@tsinghua.edu.cn.

ORCID Ⓞ
Zhen Yang: 0000-0002-8208-1638
Yingying Zhang: 0000-0002-8448-3059

Author Contributions
#Z. Yang and Y. Pang contributed equally to this work.

Notes
The authors declare no competing financial interest.

REFERENCES

(1) Pu, X.; Li, L.; Song, H.; Du, C.; Zhao, Z.; Jiang, C.; Cao, G.; Hu, W.; Wang, Z. L. A Self-Charging Power Unit by Integration of a Textile Triboelectric Nanogenerator and a Flexible Lithium-Ion Battery for Wearable Electronics. *Adv. Mater.* **2015**, *27*, 2472−2478.

(2) Rogers, J. A.; Someya, T.; Huang, Y. Materials and Mechanics for Stretchable Electronics. *Science* **2010**, *327*, 1603−1607.

(3) Kim, Y.; Zhu, J.; Yeom, B.; Di Prima, M.; Su, X.; Kim, J. G.; Yoo, S. J.; Uher, C.; Kotov, N. A. Stretchable Nanoparticle Conductors with Self-Organized Conductive Pathways. *Nature* **2013**, *500*, 59−63.

(4) Trung, T. Q.; Ramasundaram, S.; Hwang, B. U.; Lee, N. E. An All-Elastomeric Transparent and Stretchable Temperature Sensor for Body-Attachable Wearable Electronics. *Adv. Mater.* **2016**, *28*, 502−509.

(5) Wang, Y.; Wang, L.; Yang, T.; Li, X.; Zang, X.; Zhu, M.; Wang, K.; Wu, D.; Zhu, H. Wearable and Highly Sensitive Graphene Strain Sensors for Human Motion Monitoring. *Adv. Funct. Mater.* **2014**, *24*, 4666−4670.

(6) Schwartz, G.; Tee, B. C.-K.; Mei, J.; Appleton, A. L.; Kim, D. H.; Wang, H.; Bao, Z. Flexible Polymer Transistors with High Pressure Sensitivity for Application in Electronic Skin and Health Monitoring. *Nat. Commun.* **2013**, *4*, 1859.

(7) Yamada, T.; Hayamizu, Y.; Yamamoto, Y.; Yomogida, Y.; Izadi-najafabadi, A.; Futaba, D. N.; Hata, K. A Stretchable Carbon Nanotube Strain Sensor for Human-Motion Detection. *Nat. Nanotechnol.* **2011**, *6*, 296−301.

(8) Roh, E.; Hwang, B. U.; Kim, D.; Kim, B. Y.; Lee, N. E. Stretchable, Transparent, Ultrasensitive, and Patchable Strain Sensor for Human-Machine Interfaces Comprising a Nanohybrid of Carbon Nanotubes and Conductive Elastomers. *ACS Nano* **2015**, *9*, 6252−6261.

(9) Muth, J. T.; Vogt, D. M.; Truby, R. L.; Mengüç, Y.; Kolesky, D. B.; Wood, R. J.; Lewis, J. A. Embedded 3D Printing of Strain Sensors

within Highly Stretchable Elastomers. *Adv. Mater.* **2014**, *26*, 6307−6312.

(10) Hwang, B. U.; Lee, J. H.; Trung, T. Q.; Roh, E.; Kim, D. Il; Kim, S. W.; Lee, N. E. Transparent Stretchable Self-Powered Patchable Sensor Platform with Ultrasensitive Recognition of Human Activities. *ACS Nano* **2015**, *9*, 8801−8810.

(11) Ge, J.; Sun, L.; Zhang, F. R.; Zhang, Y.; Shi, L. A.; Zhao, H. Y.; Zhu, H. W.; Jiang, H. L.; Yu, S. H. A Stretchable Electronic Fabric Artificial Skin with Pressure-, Lateral Strain-, and Flexion-Sensitive Properties. *Adv. Mater.* **2016**, *28*, 722−728.

(12) Liu, Z.; Qi, D.; Guo, P.; Liu, Y.; Zhu, B.; Yang, H.; Liu, Y.; Li, B.; Zhang, C.; Yu, J.; Liedberg, B.; Chen, X. Thickness-Gradient Films for High Gauge Factor Stretchable Strain Sensors. *Adv. Mater.* **2015**, *27*, 6230−6237.

(13) Trung, T. Q.; Lee, N. E. Flexible and Stretchable Physical Sensor Integrated Platforms for Wearable Human-Activity Monitoringand Personal Healthcare. *Adv. Mater.* **2016**, *28*, 4338−4372.

(14) Cai, Y.; Shen, J.; Dai, Z.; Zang, X.; Dong, Q.; Guan, G.; Li, L. J.; Huang, W.; Dong, X. Extraordinarily Stretchable All-Carbon Collaborative Nanoarchitectures for Epidermal Sensors. *Adv. Mater.* **2017**, *29*, 1−9.

(15) Sun, Q.; Seung, W.; Kim, B. J.; Seo, S.; Kim, S. W.; Cho, J. H. Active Matrix Electronic Skin Strain Sensor Based on Piezopotential-Powered Graphene Transistors. *Adv. Mater.* **2015**, *27*, 3411−3417.

(16) Cheng, Y.; Wang, R.; Sun, J.; Gao, L. A Stretchable and Highly Sensitive Graphene-Based Fiber for Sensing Tensile Strain, Bending, and Torsion. *Adv. Mater.* **2015**, *27*, 7365−7371.

(17) Zhao, J.; Wang, G.; Yang, R.; Lu, X.; Cheng, M.; He, C.; Xie, G.; Meng, J.; Shi, D.; Zhang, G. Tunable Piezoresistivity of Nanographene Films for Strain Sensing. *ACS Nano* **2015**, *9*, 1622−1629.

(18) Hempel, M.; Nezich, D.; Kong, J.; Hofmann, M. A Novel Class of Strain Gauges Based on Layered Percolative Films of 2D Materials. *Nano Lett.* **2012**, *12*, 5714−5718.

(19) Chen, Z.; Ren, W.; Gao, L.; Liu, B.; Pei, S.; Cheng, H. M. Three-Dimensional Flexible and Conductive Interconnected Graphene Networks Grown by Chemical Vapour Deposition. *Nat. Mater.* **2011**, *10*, 424−428.

(20) Yan, C.; Wang, J.; Kang, W.; Cui, M.; Wang, X.; Foo, C. Y.; Chee, K. J.; Lee, P. S. Highly Stretchable Piezoresistive Graphene-Nanocellulose Nanopaper for Strain Sensors. *Adv. Mater.* **2014**, *26*, 2022−2027.

(21) Amjadi, M.; Pichitpajongkit, A.; Lee, S.; Ryu, S.; Park, I. Highly Stretchable and Sensitive Strain Sensor Based on Silver Nanowire-Elastomer Nanocomposite. *ACS Nano* **2014**, *8*, 5154−5163.

(22) Barlian, B. A. A.; Park, W.; Mallon, J. R.; Rastegar, A. J.; Pruitt, B. L. Semiconductor Piezoresistance for Microsystems. *Proc. IEEE* **2009**, *97*, 513−552.

(23) Li, X.; Zang, X.; Li, Z.; Li, X.; Li, P.; Sun, P.; Lee, X.; Zhang, R.; Huang, Z.; Wang, K.; Wu, D.; Kang, F.; Zhu, H. Large-Area Flexible Core-Shell Graphene/Porous Carbon Woven Fabric Films for Fiber Supercapacitor Electrodes. *Adv. Funct. Mater.* **2013**, *23*, 4862−4869.

(24) Xiao, X.; Yuan, L.; Zhong, J.; Ding, T.; Liu, Y.; Cai, Z.; Rong, Y.; Han, H.; Zhou, J.; Wang, Z. L. High-Strain Sensors Based on ZnO Nanowire/Polystyrene Hybridized Flexible Films. *Adv. Mater.* **2011**, *23*, 5440−5444.

(25) Malard, L. M.; Pimenta, M. A.; Dresselhaus, G.; Dresselhaus, M. S. Raman Spectroscopy in Graphene. *Phys. Rep.* **2009**, *473*, 51−87.

(26) Ferrari, A. C. Raman Spectroscopy of Graphene and Graphite: Disorder, Electron-Phonon Coupling, Doping and Nonadiabatic Effects. *Solid State Commun.* **2007**, *143*, 47−57.

(27) Nanda, S. S.; Kim, M. J.; Yeom, K. S.; An, S. S. A.; Ju, H.; Yi, D. K. Raman Spectrum of Graphene with Its Versatile Future Perspectives. *TrAC, Trends Anal. Chem.* **2016**, *80*, 125−131.

(28) Pang, Y.; Tian, H.; Tao, L.; Li, Y.; Wang, X.; Deng, N.; Yang, Y.; Ren, T. L. Flexible, Highly Sensitive, and Wearable Pressure and Strain Sensors with Graphene Porous Network Structure. *ACS Appl. Mater. Interfaces* **2016**, *8*, 26458−26462.

(29) Li, Y.; Huang, P.; Zhu, W.; Fu, S.; Hu, N.; Liao, K. Flexible Wire-Shaped Strain Sensor from Cotton Thread for Human Health and Motion Detection. *Sci. Rep.* **2017**, *7*, 45013.

(30) Wang, D.-Y.; Tao, L.-Q.; Liu, Y.; Zhang, T.-Y.; Pang, Y.; Wang, Q.; Jiang, S.; Yang, Y.; Ren, T.-L. High Performance Flexible Strain Sensor Based on Self-Locked Overlapping Graphene Sheets. *Nanoscale* **2016**, *8*, 20090−20095.

(31) Yang, Z.; Wang, D. Y.; Pang, Y.; Li, Y. X.; Wang, Q.; Zhang, T. Y.; Wang, J. B.; Liu, X.; Yang, Y. Y.; Jian, J. M.; Jian, M. Q.; Zhang, Y. Y.; Yang, Y.; Ren, T. L. Simultaneously Detecting Subtle and Intensive Human Motions Based on a Silver Nanoparticles Bridged Graphene Strain Sensor. *ACS Appl. Mater. Interfaces* **2018**, *10*, 3948−3954.

(32) Bae, S. H.; Lee, Y.; Sharma, B. K.; Lee, H. J.; Kim, J. H.; Ahn, J. H. Graphene-Based Transparent Strain Sensor. *Carbon* **2013**, *51*, 236−242.

(33) Wang, X.; Gu, Y.; Xiong, Z.; Cui, Z.; Zhang, T. Silk-Molded Flexible, Ultrasensitive, and Highly Stable Electronic Skin for Monitoring Human Physiological Signals. *Adv. Mater.* **2014**, *26*, 1336−1342.